Deep structural imaging in the Vienna basin

Ahmed Mamdouh[1], Klaus Pelz[2], Sandor Bezdan[2], Erika Angerer[2], Alexandra Oteleanu[2], Harald Granser[2], Abdelrahman Abubakr[1], Alexander Sakharov[3] and Ian F. Jones[1]*

Abstract

Reprocessing of a recent wide azimuth vibroseis survey in the Vienna basin, followed by detailed anisotropic velocity model building and pre-stack depth migration, has led to an improved understanding of the subsurface structure, helping to de-risk future drilling decisions. Several processing and imaging routes were investigated, including common reflection surface stacking, 5D regularisation, Kirchhoff and common reflection angle migrations, using an interpretation-constrained velocity model. Results for the different routes are compared, with an assessment of the interpretational uplift obtained with the different approaches.

Introduction

The Vienna basin is a mature and well established gas-producing region, with current production from the relatively simple, shallow flat-lying Neogene section and the more structurally complex pre-Neogene section, at depths greater than 3 km.

Previous studies, combining gravity and seismic information (Granser, 1987; Rossi et al., 1998; Vesnaver et al., 2000; Spitzer and Gierse, 2008; Pfeiler et al., 2011; Salcher et al., 2012; Pelz et al., 2018; Garden and Zühlsdorff, 2019; Šamajová et al., 2019; Harzhauser et al., 2022) have outlined the overall structural picture of the Vienna basin, but obtaining the detail required for accurate deep well placement remains problematic. In addition, the recent interest in carbon capture and storage and CO_2 enhanced oil recovery has led to further investigation to identify structures suitable for these purposes (e.g. Mikunda et al., 2020). Figure 1 shows a tectonic overview (Garden and Zühlsdorff, 2019 as adapted from Wessely, 1992): as can be inferred, whereas the Neogene shallow section (extending to a depth of approximately 3 km), is structurally simple, the deeper pre-Neogene section is extremely complex, combining regional thrust faults with highly distorted overturned beds.

The data used for this study were acquired between 2017 and 2019 as part of a large wide azimuth survey over the Schönkirchen area using a Vibroseis source, emphasising the low frequencies to help with deep imaging. For most of the survey, the sweep range used was 2 Hz-90 Hz, with a 64 s sweep producing 9 s

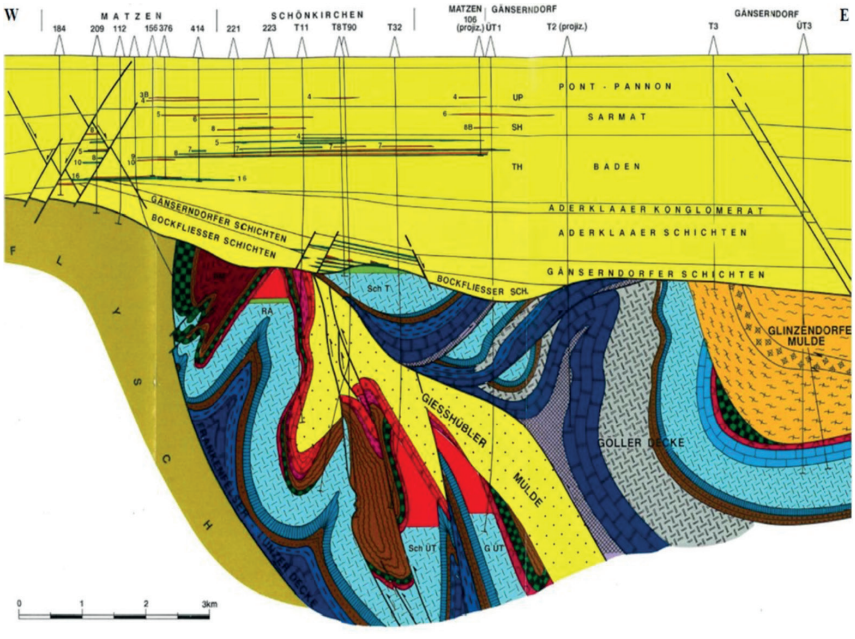

Figure 1 Tectonic overview. Geological section of the Vienna Basin. Wells drilled by the time the section was produced are indicated. Most of the wells target shallow, thin reservoirs within the Neogene sands (yellow). Green indicates oil reservoirs, red indicates gas reservoirs, known or expected. The deep carbonate reservoirs (hashed light blue) are of exploration interest.

[1] Brightskies Geoscience | [2] OMV, Vienna | [3] SeisEdge, Stavanger
* Corresponding author, E-mail: Ian.Jones@bsgeoscience.com
DOI: 10.3997/1365-2397.fb2023097

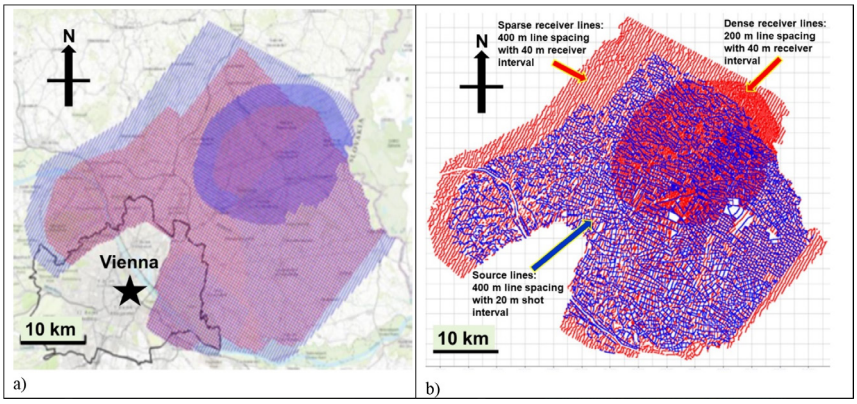

Figure 2 Survey area, showing the location relative to Vienna (a), and indicating different phases of the acquisition (b). In 2b, the denser red area had a finer 200 m receiver line spacing, compared to the 400 m spacing over the rest of the area.

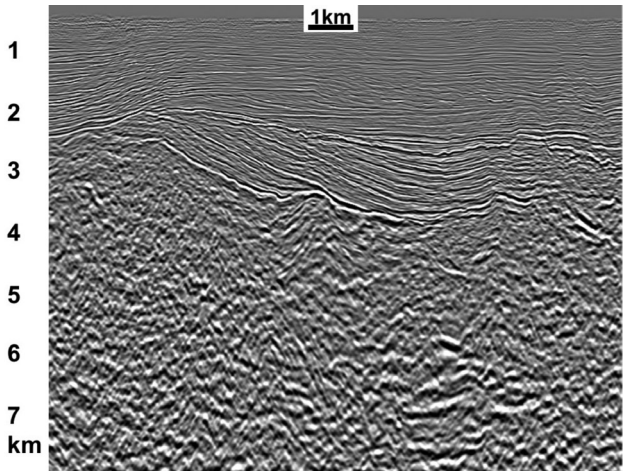

Figure 3 Vintage preSDM image from the 2020 processing, showing the full section. Although the shallow pre-Neogene section (down to approximately 3 km) is well imaged, the deeper structural image is still ambiguous.

records (in urban areas, a 12 Hz low-end of the sweep had to be used). These data were initially processed between 2018 and 2020 as part of a project that also incorporated some earlier vintage data (acquired in 2016) covering an area of about 1500 km^2. In the study presented here, only a 500 km^2 subset of the recent wide azimuth Vibroseis data were used. Figure 2 shows a location map, indicating the different phases of acquisition. Most of the area was shot with 400 m receiver line spacing with 40 m receiver interval, and 400 m shot line spacing with 20 m shot interval, but the denser red area in Figure 2b has denser 200 m receiver line spacing.

Methodology

The anisotropic velocity model for the overburden Neogene sedimentary sequence had been adequately constructed in the previous 2020 processing project using a combination of first-arrival refraction tomography and subsequent reflection tomography. In this phase of the study we concentrated on the more problematic, structurally complex pre-Neogene sequence. At these depths (typically greater than 3 km) are found the highly deformed nappes of the Northern Calcareous Alps (NCA) formed during an active tectonic period in the Late Cretaceous period.

In the earlier processing project that focused on the shallower geological section, the processing parameters were optimised for high resolution shallower imaging, and not for preservation of the deeper structure. Hence, in the work considered here, the pre-processing was repeated optimising parameters for the deeper, pre-Neogene section. Overall, the parameterisation of the many and various noise suppression methods was selected to be milder than in the original processing in order to better preserve the signal content of the pre-Neogene section. Figure 3 shows a final image from the 2020 project showing good shallow imaging of the mostly flat-lying Neogene structures.

Both 5D regularisation and common reflection surface processing (CRS) were assessed, and the CRS data selected as input for anisotropic Kirchhoff migration, as it preserved the deeper signal more than the 5D approach. Azimuth information was preserved during OVT processing to assess any azimuthal velocity variation.

An initial pass of (ray-based) anisotropic tomographic inversion was performed, to optimise gather flatness using the available offsets (a maximum of ~8 km, but more generally about 6 km), and to refine the anisotropy parameters. The delta values were updated by calibrating against the available well-control, and epsilon adjusted during the tomographic inversion, resulting in delta values of about 4% down to 1 km, 9% from 1 km - 2.5 km, and decreasing to around 2% in the pre-Neogene section, with epsilon ~1.5*delta. For the three main wells in the target area, the resulting misties at around 3600 m depth were: -20 m, 0 m, and +10m. Thereafter a migration-scanning approach followed by automated identification of the most coherent elements of the scanned images was used to update the velocity model. Two passes of scanning were performed initially perturbing the tomographic velocity field from 91% to 109% in steps of 3%, with a second pass starting from the output model from pass #1, perturbing that model between 96% and 106% in steps of 2%. Following this, a reflectivity-based geobody insertion method was used to adjust the velocities in the regions where high velocity dolomite rafts were believed to exist. This method relied on the instantaneous phase of high reflectivity events, constrained with well-control to determine the geobody velocities (Valler et al., 2017).

Results

Figure 4 outlines the evolution of the velocity model starting from the 2020 legacy anisotropic model which can be seen to be lacking in any structural detail in the deeper section. After an initial

pass of tomographic inversion updating only velocity, the model was recalibrated against the well-database to facilitate an update of delta, followed by recalibration of the epsilon parameter to maintain gather flatness (higher order moveout was not visible on the gathers in the deeper section). In migrations using the final anisotropic velocity model, the depth mis-ties at the pre-Neogene level (depth ~3600 m) in the three wells in the target area were 0 m, 10 m, and -20 m.

Kirchhoff 3D depth migration with an intermediate velocity model on the relatively raw field data already showed better preservation of the target events (Figure 5). The dipping event outlined in the yellow ellipse is known to be a real event

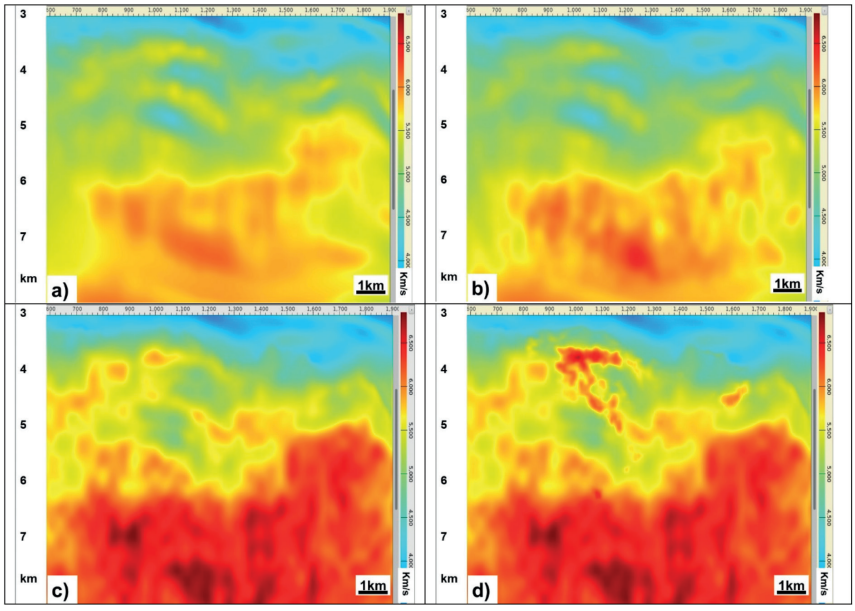

Figure 4 a) legacy anisotropic velocity model; b) anisotropic velocity field following initial tomographic update and recalibration to wells, c) velocity after scanning and automated update; d) final velocity field after high contrast geobody insertion for the dolomite rafts.

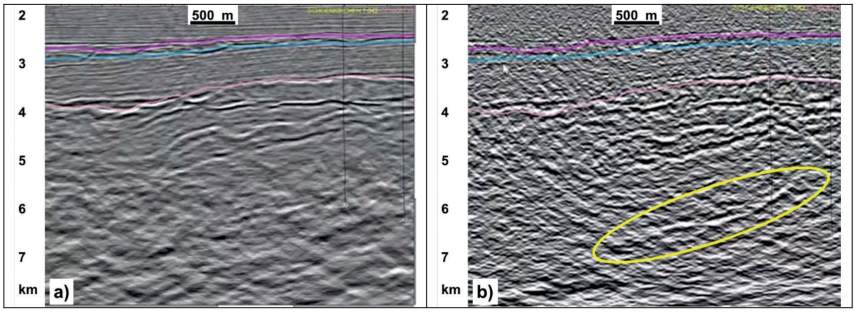

Figure 5 Zoom on the target area, comparing an inline from the final vintage 2020 processing a) and an early stage image from the new processing before denoise and final model update. The target event (outlined in the yellow ellipse) is more clearly visible in the new (but still noisy) image. The vintage image has good resolution of the shallow section and is 'clean' but has degraded the integrity of the deeper target structure.

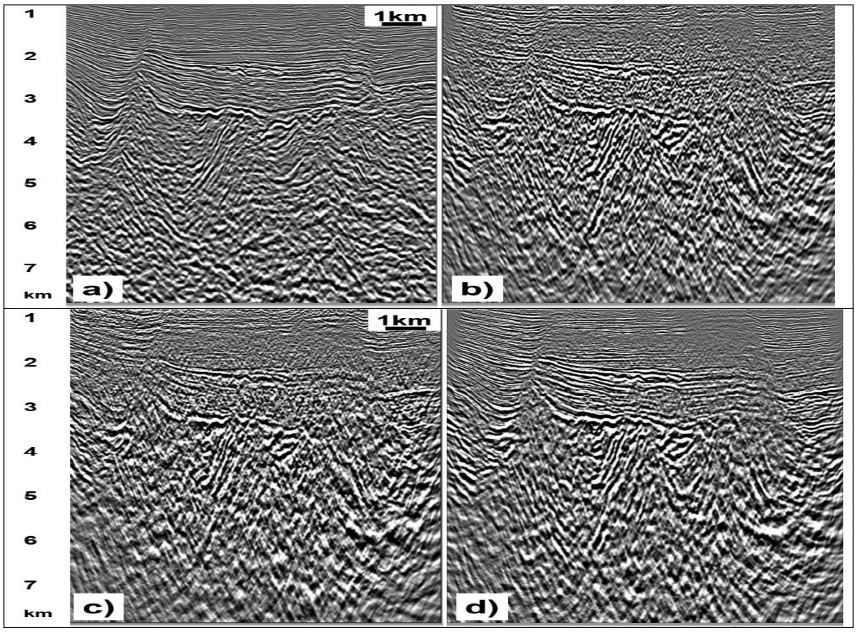

Figure 6 Crossline comparing a) vintage result from 2020 processing; b) new denoised processing with final model; c) 5D regularisation with final model; d) CRS input with final model. The 5D regularisation has slightly degraded some of the very deepest structures, hence the CRS result was preferred. In the CRS result (d) it can clearly be seen that the steep dip fault planes and other structural elements are much better preserved than in the vintage data (a).

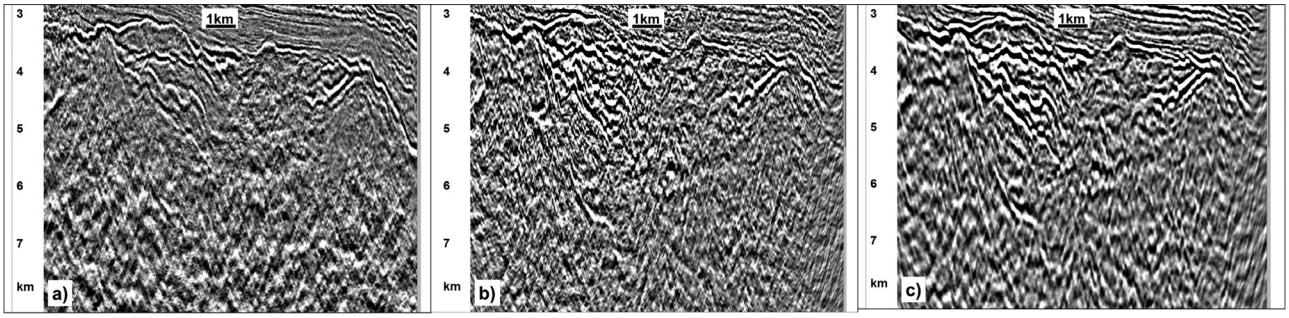

Figure 7 Zoom on the deeper target structure comparing a) the 2020 vintage preSDM; b) preSDM from the current project using the reprocessed input data and final geobody velocity model with structurally orientated smoothing applied to the resulting image; c) and the reprocessed input data with additional CRS processing. This is the line for which the velocities were shown in Figure 4.

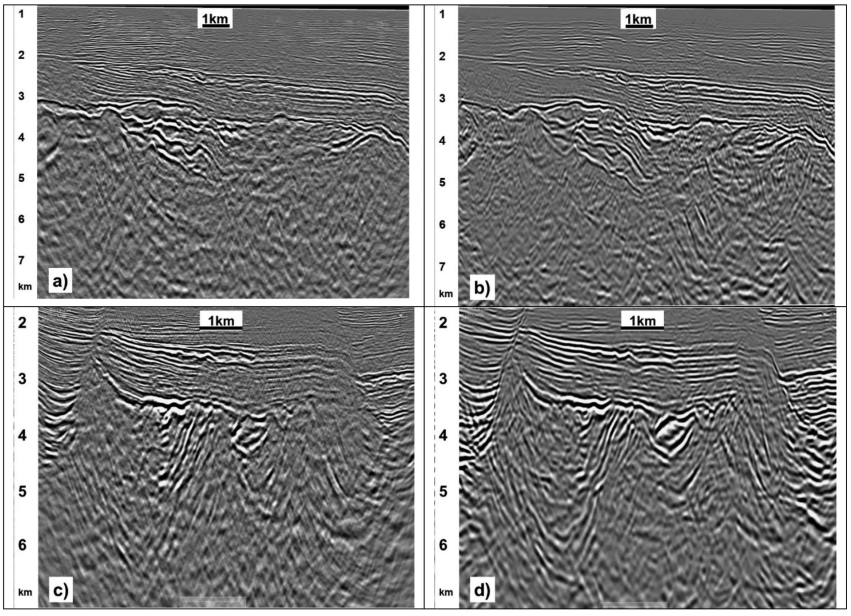

Figure 8 Zoom on the deeper target structure comparing a) Kirchhoff preSDM inline from the current project using the reprocessed input data with additional CRS processing, b) CRAM preSDM inline, c) Kirchhoff CRS crossline, d) CRAM crossline. For the most-part, the CRAM result clearly improves the steeply dipping events and fault planes, as well as suppressing noise.

(from well penetrations) and is better preserved in the new data processing, even before application of additional denoise procedures. Figure 6 shows a central crossline comparing the newly processed data migrated with the final geobody model for three denoise and interpolation strategies and contrasts these results with the corresponding vintage 2020 image. Figure 6a is the preSDM of the vintage data, Figure 6b is the migration of the basic denoise data, Figure 6c is the migration after 5D regularisation/interpolation, and Figure 6d is the migration of CRS processed data. The 5D regularisation has slightly degraded some of the very deepest structures, hence the CRS result was preferred for interpretation.

Figure 7 shows an inline through the target area comparing the vintage result with Kirchhoff preSDM images produced with the newly denoised data and the CRS processed data. Again, the vintage result is suboptimal in the deep section. In addition to the Kirchhoff migration, a common reflection angle migration (CRAM) was performed. CRAM performs its ray-tracing directly from the subsurface and with respect to the subsurface dip field, so is usually better able to suppress migration noise than a conventional Kirchhoff scheme. Overall, this gave a significant uplift in terms of signal to noise, with improved imaging of most of the steeply dipping events (Figure 8).

Discussion

The success of OMV's upcoming drilling programme in the Vienna Basin depends to a large extent on a reliable interpretation of the deep pre-Neogene structure from seismic images. Seismic data from this area are known to be of notoriously poor quality in terms of the signal-to-noise ratio of the deeper section. Hence, here we strove to be extremely cautious in the application of various de-noise procedures so as not to compromise any weak underlying signal: the emphasis being on retaining as much signal as possible, guided by the knowledge of dips and locations of various structural elements obtained from well logs. Being able to better understand both the basin architecture and the faulting and compartmentalisation of the reservoir units was central to de-risking the prospectivity of the area.

Based on the images obtained during this reworking of the recent data, we have been able to advance our knowledge with sufficient confidence to guide the infill drilling programme. OMV's recent natural gas discovery in this area (the largest in Austria for 40 years), confirmed with the successful Wittau Tief-2a exploration well, points to the importance of this prospect, and the new imaging presented in this study should help with future appraisal well drilling.

Acknowledgements

We would like to thank Oliver Langton and Paul Keane for helpful suggestions on improvements to the paper, AspenTech for provision of the Common Reflection Angle Migration software, and to OMV E&P GmbH for permission to publish this work. We would also like to thank Gwenola Michaud the other reviewers for their constructive and helpful suggestions.

References

Garden, M. and Zühlsdorff, L. [2019]. Acquisition of a modern seismic survey in the Vienna Basin, SEG annual.

Granser, H. [1987], Three-dimensional interpretation of gravity data from sedimentary basins using an exponential density-depth function, *Geophys. Prospect*., **35**, 1030–1041.

Harzhauser, M., Kranner, M., Mandic, O., ´Cori´c, S. and Siedl, W., [2022]. High resolution Late Miocene sediment accommodation rates and subsidence history in the Austrian part of the Vienna Basin, *Marine and Petroleum Geology,* 145 (2022) 105872.

Mikunda, T., Franců, J., Pereszlényi, M., Hladík, V., Kolejka, V., Kulich, J., Götzl, G., Kollbotn, L. and Jankulár, M. [2020]. Report: *Towards a strategic development plan for CO2-EOR in the Vienna Basin*. European Union Horizon 2020 research and innovation programme under grant agreement No 653718, ENOS, http://www.enos-project.eu.

Pelz, K., Granado, P., Strauss, P., Roca, E., König, M., Thöny, W., Peresson, H. and Muñoz, J.A. [2018]. Overturned to recumbent thrust sheets in the Northern Calcareous Alps (NCA)—The role of inflated salt on fold-and-thrust belt structural styles: *EGU General Assembly Conference Abstracts 20*, 7676.

Pfeiler, S., Fuchsluger, M., Stotter, C., Chwatal, W. and Brückl, E. [2011]. *3D Model Based Acquisition Design for Imaging the Deep Vienna Basin*. Eage Annual Conference.

Rossi, G., Böhm, G., Madrussani, G., Vesnaver, A., and Granser, H. [1998]. *3D adaptive tomography and imaging in the Vienna Basin*, SEG annual.

Salcher, B.C., Meurers, B., Smit, J., Decker, K., Hölzel, M. and Wagreich, M. [2012]. Strike-slip tectonics and Quaternary basin formation along the Vienna Basin fault system inferred from Bouguer gravity derivatives, *Tectonics* , **31**, TC3004, doi:10.1029/2011TC002979.

Šamajová, L., Hák, J., Csibri, T., Bielik, M., Teták, F., Brixová, B., Sliva, L. and Šály, B. [2019]. Geophysical and geological interpretation of the Vienna Basin pre-Neogene basement (Slovak part of the Vienna Basin). *Geologica Carpathia*, **70**(5), 418-431.

Spitzer, R. and Gierse, G. [2008]. *Target-oriented Seismic Data Processing in the Vienna Basin – A Key to Improve Imaging Using Vintage Data*, EAGE Annual Conference.

Valler, V., Nathan Payne, N., Hallett, T., Kobylarski, M., Venkatraman, G., Rappke, J. and Fairclough, D. [2017]. A holistic approach to model-building in and around injectites: a case-study offshore Norway, Eage Annual Conference.

Vesnaver, A., Böhm, G., Madrussani, G., Rossi, G. and Granser, H. [2000]. Depth imaging and velocity calibration by 3D adaptive tomography. *First Break*, **18**, 303-312.

Wessely, G. [1992]. The Calcareous Alps below the Vienna Basin in Austria and their structural and facial development in the Alpine-Carpathian border zone: *Geologica Carpathica*, **43**, 347-353.